UNIVERSITY
OF WOLLONGONG
AUSTRALIA

University of Wollongong
Research Online

Faculty of Engineering and Information Sciences - Papers: Part B

Faculty of Engineering and Information Sciences

2018

Microdosimetric applications in proton and heavy ion therapy using silicon microdosimeters

Lachlan Chartier
University of Wollongong, lc752@uowmail.edu.au

Linh T. Tran
University of Wollongong, tltran@uow.edu.au

David Bolst
University of Wollongong, dbolst@uow.edu.au

Susanna Guatelli
University of Wollongong, susanna@uow.edu.au

Alex Pogossov
University of Wollongong

See next page for additional authors

Publication Details

Chartier, L., Tran, L. T., Bolst, D., Guatelli, S., Pogossov, A., Prokopovich, D. A., Reinhard, M. I., Perevertaylo, V., Anderson, S., Beltran, C., Matsufuji, N., Jackson, M. & Rosenfeld, A. B. (2018). Microdosimetric applications in proton and heavy ion therapy using silicon microdosimeters. Radiation Protection Dosimetry, 180 (1-4), 365-371.

Research Online is the open access institutional repository for the University of Wollongong. For further information contact the UOW Library: research-pubs@uow.edu.au

Microdosimetric applications in proton and heavy ion therapy using silicon microdosimeters

Abstract

Using the CMRP 'bridge' μ+ probe, microdosimetric measurements were undertaken out-of-field using a therapeutic scanning proton pencil beam and in-field using a ^{12}C ion therapy field. These measurements were undertaken at Mayo Clinic, Rochester, USA and at HIMAC, Chiba, Japan, respectively. For a typical proton field used in the treatment of deep-seated tumors, we observed dose-equivalent values ranging from 0.62 to 0.99 mSv/Gy at locations downstream of the distal edge. Lateral measurements at depths close to the entrance and along the SOBP plateau were found to reach maximum values of 3.1 mSv/Gy and 5.3 mSv/Gy at 10 mm from the field edge, respectively, and decreased to ~0.04 mSv/Gy 120 mm from the field edge. The ability to measure the dose-equivalent with high spatial resolution is particularly relevant to healthy tissue dose calculations in hadron therapy treatments. We have also shown qualitatively and quantitively the effects critical organ motion would have in treatment using microdosimetric spectra. Large differences in spectra and RBE_{10} were observed for treatments where miscalculations of ^{12}C ion range would result in critical structures being irradiated, showing the importance of motion management.

Disciplines

Engineering | Science and Technology Studies

Publication Details

Chartier, L., Tran, L. T., Bolst, D., Guatelli, S., Pogossov, A., Prokopovich, D. A., Reinhard, M. I., Perevertaylo, V., Anderson, S., Beltran, C., Matsufuji, N., Jackson, M. & Rosenfeld, A. B. (2018). Microdosimetric applications in proton and heavy ion therapy using silicon microdosimeters. Radiation Protection Dosimetry, 180 (1-4), 365-371.

Authors

Lachlan Chartier, Linh T. Tran, David Bolst, Susanna Guatelli, Alex Pogossov, Dale A. Prokopovich, Mark I. Reinhard, Vladimir Perevertaylo, Sarah Anderson, Chris Beltran, Naruhiro Matsufuji, Michael A. Jackson, and Anatoly B. Rosenfeld

This journal article is available at Research Online: https://ro.uow.edu.au/eispapers1/2172

MICRODOSIMETRIC APPLICATIONS IN PROTON AND HEAVY ION THERAPY USING SILICON MICRODOSIMETERS

L. Chartier[1], L. T. Tran[1], D. Bolst[1], S. Guatelli[1], A. Pogossov[1], D. A. Prokopovich[1,2], M. I. Reinhard[1,2], V. Perevertaylo[3], S. Anderson[4], C. Beltran[4], N. Matsufuji[5], M. Jackson[1,6], and A. B. Rosenfeld[1,*]
[1]Centre for Medical Radiation Physics, University of Wollongong, Wollongong, NSW, 2522, Australia
[2]Ionising Radiation, Nuclear Stewardship Platform, NSTLI, ANSTO, Lucas Heights, NSW, 2234, Australia
[3]SPA-BIT, Kiev, Ukraine
[4]Department of Radiation Oncology, Mayo Clinic, Rochester, MN 55902, USA
[5]National Institute for Quantum and Radiological Science and Technology, Japan
[6]School of Medicine, University of New South Wales, Kensington, NSW, 2052, Australia

Using the CMRP "bridge" μ^+ probe, microdosimetric measurements were undertaken out-of-field using a therapeutic scanning proton pencil beam and in-field using a ^{12}C ion therapy field. These measurements were undertaken at Mayo Clinic, Rochester, USA and at HIMAC, Chiba, Japan, respectively. For a typical proton field used in the treatment of deep-seated tumors, we observed dose-equivalent values ranging from 0.62-0.99 mSv/Gy at locations downstream of the distal edge. Lateral measurements at depths close to the entrance and along the SOBP plateau were found to reach maximum values of 3.1 mSv/Gy and 5.3 mSv/Gy at 10mm from the field edge, respectively, and decreased to approximately 0.04 mSv/Gy 120 mm from the field edge. The ability to measure the dose-equivalent with high spatial resolution is particularly relevant to healthy tissue dose calculations in hadron therapy treatments. We have also shown qualitatively and quantitively the effects critical organ motion would have in treatment using microdosimetric spectra. Large differences in spectra and RBE_{10} were observed for treatments where miscalculations of ^{12}C ion range would result in critical structures being irradiated, showing the importance of motion management.

INTRODUCTION

Delivery of dose to out-of-field healthy tissue is always detrimental to treatment outcome across all radiation therapy modalities, and naturally increases the risk of secondary malignancy, especially in children[(1)]. The ions used in charged particle therapy undergo interactions with materials in the beam line, treatment head, beam-shaping devices and within the patient. Unlike most conventional photon therapies, these interactions are both electronic *and* nuclear in nature. While most processes are due to multiple Coulomb scattering, reactions with target nuclei can generate neutrons and fragments that will deliver excess dose to both target and non-target regions distally and laterally within a patient[(2)]. Naturally, the absence of materials upstream of the patient reduces neutron and fragment production and is one of many reasons why particle therapy modalities are moving from passive scattering to active scanning techniques to deliver and shape the beam to the target[(3,4)].

Many studies with protons have been undertaken to measure the out-of-field dose delivered to tissue external to the target volume[(5-9)], however due to differing measuring techniques, beam geometries, proton energies and acquisition locations, it is difficult to compare them directly. Furthermore, most measurements are taken around the room, far outside the patient which is not particularly relevant to treatment outcomes. Whilst there can be large differences in delivery systems and in-beam devices, most studies obtained similar dose-equivalent values up to the order of 10 mSv/Gy close to the field, and decreasing to minima of between 0.001 - 0.1 mSv/Gy at distances of 10-100 cm lateral to the field. Due to the absence of beam modifying materials, active scanning systems produce less neutrons and as a result, lower dose-equivalent values, however the extent to which this is true has been disputed in the past[(10,11)].

One factor that can affect the dose delivered to the treatment volumes and out-of-field regions of the body is intra-fractional organ motion. This is true for all treatment types, however it is especially important in particle therapy due to increased relative biological effectiveness (RBE) at the Bragg peak caused by high LET particles. Respiratory motion is one type of motion that causes decreased treatment efficiency as it not only affects the ability to accurately treat lung cancer, it also causes other organs in the body to move from their predicted locations[(12)]. This can cause large

*Corresponding author: anatoly@uow.edu.au

errors in delivered dose to the tumor, healthy tissue and critical organs, especially if close to the Bragg peak. Whilst preliminary theoretical calculations and cell studies have been undertaken to investigate motion in particle therapy[13], the effect that organ motion has on particle spectra and the RBE needs further investigation, especially with advancing technology such as proton and ^{12}C pencil beam scanning systems.

One technique that can be utilized to evaluate both out-of-field and in-field quality of mixed radiation fields is microdosimetry. It can be used for radiation protection purposes to calculate dosimetric quantities such as the out-of-field dose-equivalent, as well as the RBE in therapeutic fields, based on radiobiological models. Using the radiological modified microdosimetric kinetic model (MKM) and microdosimetric spectra[14], RBE_{10} can be derived, defined as the ratio of the dose required to achieve 10% cell survival using X-rays to that required when using the radiation of interest. The fundamental quantity used in microdosimetry is the lineal energy y, defined in equation 1, with units keV/μm[15]. To measure lineal energy, a detector is required that can measure single energy deposition events of magnitude E and possess geometry with a well-known average chord length $\bar{l}$. The dose-mean lineal energy $\overline{y_D}$, defined as the first moment of its dose-weighted distribution $d(y)$ (eqation 2), can be used to describe the field at a specific point using the distribution of lineal energy events $f(y)$.

$$y = E/\bar{l} \quad (1)$$

$$d(y) = yf(y)/\int yf(y)dy \quad (2)$$

Previous work with silicon microdosimeters has been undertaken by the CMRP to measure microdosimetric quantities in-field[16] and out-of-field[17, 18] in passively scattered proton fields, however studies have not been carried out using proton pencil beam scanning (PBS). This work demonstrates the usefulness of new silicon-on-insulator (SOI) microdosimeters in assessing beam quality in proton PBS and ^{12}C ion therapy systems. The dose-equivalent and other microdosimetric quantities have been determined in out-of-field locations using a spread-out Bragg peak proton PBS field at Mayo Clinic, Rochester, USA. We also present work undertaken at the Heavy Ion Medical Accelerator in Chiba (HIMAC), Japan to investigate the effect that motion has on microdosimetric spectra and RBE_{10} in a typical patient plan using passive beam delivery.

METHODS

SOI Bridge Microdosimeter

The Bridge microdosimeter is a segmented SOI radiation detector containing 4248 PIN diodes, referred to as sensitive volumes (SVs). Each SV has an area of 30×30 μm^2 and thickness 10 μm in order approximate the size of mammalian cells. To prevent external charge collection to the SVs and improve its geometric definition, the silicon surrounding the diodes has been removed using plasma etching, leaving well-defined parallelepiped SVs with 20 x 15 x 10 μm "bridges" that support the aluminium bus. The microdosimeter is packaged on an in-house designed front-end probe, known as the MicroPlus (μ^+) probe, created to minimize noise associated with leakage current and capacitance at the microdosimeters operating voltage (10V), seen in figure 1. The Bridge microdosimeter has been described and characterized in terms of its charge collection in previous works[17, 18].

The μ^+ probe is placed in a waterproof PMMA sheath to protect the electronics and allow operation in a water phantom. Attached to the μ^+ probe is an in-house designed shaping amplifier which converts the preamplifier pulse to a Gaussian for processing by an Amptek multichannel analyzer (MCA).

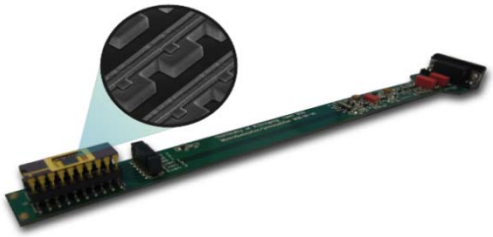

Figure 1. μ^+ probe with SEM image showing the Bridge Microdosimeter sensitive volumes.

Phantom

Previous studies have used a modular PMMA phantom to adjust the microdosimeter depth, however this setup is relatively inflexible due to the set thickness of PMMA slabs. To overcome this limitation, a relatively low-cost XY-stage was built using a MakerBot Replicator 3D-printer and PMMA water tank, controlled remotely using Arduino-driven stepper motors. Not only does such a system allow flexibility in controlling the depth and lateral position of the microdosimeter, it also facilitates custom movements, used in this study to simulate simple linear motion as well as lung motion. This is achieved by moving the depth and lateral position of the detector using predefined profiles.

Out-of-field PBS measurements at Mayo Clinic

Out-of-field measurements were undertaken to investigate radiation effects that would occur in healthy tissue surrounding a treatment volume. This was carried out at the proton therapy facility at Mayo Clinic Hospital, Rochester, MN, USA. This system employs intensity modulated PBS to deliver treatment without the use of patient-specific beam shaping devices. A 2.2 Gy treatment was delivered as a 10 x 10 cm^2 SOBP field with 6cm modulation between 40-100mm, created

using proton energy layers between 71.3 - 118.4 MeV. The depth-dose profile along the central axis of the field is shown in figure 2.

Measurements were taken laterally at 10, 30, 60 and 120 mm from the field edge at depths close to the beam entrance (25 mm) and on the plateau region of the SOBP (80 mm). In addition, two locations downstream of the distal edge of the SOBP (110 and 150 mm depths) were also investigated.

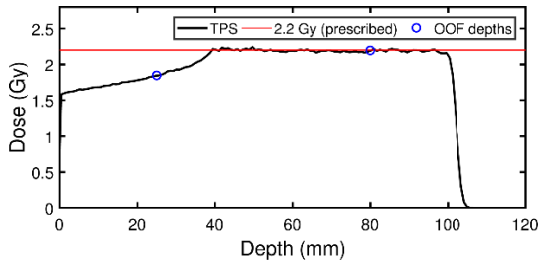

Figure 2. Depth-dose profile of the PBS proton SOBP field, calculated using the Mayo Clinic Geant4 GPU treatment planning system (TPS). Out-of-field (OOF) depths represent the depths of lateral acquisitions.

Dose-equivalent Determination

The dose-equivalent H is defined as the product of the absorbed dose and a quality factor and is used to estimate the dose received by a person upon radiation exposure. Using the lineal energy dependent quality factor $Q(y)$, defined in the ICRU-40 report[19] for radiation protection, the dose is scaled to be proportional to the biological effects it causes with respect to effects produced by a reference radiation. The method for calculating the dose-equivalent using microdosimetry is explained in detail in previous work[8]. Based on more accurate Geant4 simulations done recently, a conversion factor of $\zeta = 0.58$ is used to convert dose in the silicon sensitive volumes to tissue-equivalent sensitive volumes[20].

Geant4 Simulations

The PBS delivery at Mayo Clinic was modeled using Geant4 version 10.2p2. The positional sigma of the beam was calculated based on the starting combination of energy and position, with the FWHM value ranging between 6-16.5 mm. The phantom was modelled as a slab of 40 × 40 × 30 cm^3 water placed in air 80 cm away from the beam nozzle. The response of the bridge microdosimeter from being irradiated by the SOBP was simulated, with identical physics options as adopted in[21].

Motion Effects Study in Heavy Ion Therapy at HIMAC

Experiments were performed at the Heavy Ion Medical Accelerator in Chiba, NIRS, Japan, utilizing a passively scattered ^{12}C ion beam to irradiate the microdosimeter. A 10 × 10 cm^2 field with a 6cm SOBP and maximum energy of 290 MeV/u was created with a ridge filter. The microdosimeter was placed at the distal edge of the SOBP along the beam's central axis.

The effect of lung motion on a hypothetical critical organ which is ideally located downstream of the SOBP was investigated. This scenario occurs due to a particle range miscalculation from a lack of motion management, leading to the critical structure moving between 7 mm upstream (in-field) and 1 mm downstream, in the same trajectory that a real lung would travel. This was achieved by placing the microdosimeter at the end of the SOBP and obtaining microdosimetric spectra at the point of interest when stationary 1 mm downstream and while undergoing a lung motion profile (captured from 4D CT data) within the phantom as mentioned above.

In addition to critical organ modeling, changes to microdosimetric quantities within a spherical treatment volume when introducing motion were investigated. A laterally changing particle field was produced using a spherical polyethylene bolus, placed upstream along the central axis of the beam. The microdosimeter was positioned at various off-axis locations in the water tank, labelled A and B in figure 3. A linear motion profile was applied at each location, moving it from 20 mm to 40 mm off-axis, towards the edge of the bolus.

For all motion configurations, microdosimetric spectra were obtained at stationary positions and while undergoing motion. Using the spectra, the dose-mean lineal energy $\overline{y_D}$ was determined, as well as the RBE_{10} calculated using the MKM model, as described in previous work [14,17,18].

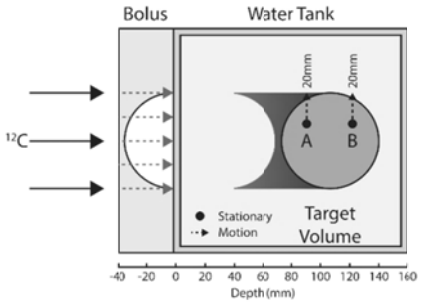

Figure 3. Schematic showing the phantom-bolus setup with acquisition points (A, B), and motion vectors.

Uncertainties

Uncertainty in the spectra and associated quantities is based on the statistical error associated with the counts in each MCA channel. Errors in $\overline{y_D}$, $\bar{Q}$, H and RBE_{10} were determined using standard error propagation techniques, and are again dependent on the counts in each channel of the MCA spectra. Maximum

uncertainty in depth and lateral position of the microdosimeter is at most 1 mm, based on the repeatability of movement and measurement of the initial microdosimeter position. There is an inherent uncertainty in the silicon-to-tissue conversion factor ζ of approximately 2%.

RESULTS

Out-of-Field Measurements using Proton PBS

Downstream of the SOBP

Table. 1 presents the dose-mean lineal energy $\overline{y_D}$, average quality factor $\bar{Q}$ and dose-equivalent H from acquisitions located downstream at depths of 110mm and 150mm, with corresponding microdosimetric spectra shown in figure 4. The generation of higher LET particles is seen to be more prevalent at 150 mm as can be seen by higher $\overline{y_D}$ and $\bar{Q}$ values, however H is lower, resulting in less dose delivered out-of-field from neutrons, per treatment Gy. In both spectra, high LET events above 100 keV/μm are most likely from alpha particles produced through (n, α) inelastic reactions within the silicon, carbon and oxygen. Despite these events, the spectra is mainly dominated by lower lineal energy events originating from recoil protons produced through elastic (n,p) reactions inside the water phantom.

Table 1. Dose-mean lineal energy, average quality factor and dose-equivalent for downstream acquisitions

Depth (mm)	$\overline{y_D}$ (keV/μm)	$\bar{Q}$	H/Dose (mSv/Gy))
110	21.9 ± 3.4	5.4 ± 0.6	0.99 ± 0.11
150	27.2 ± 5.7	6.1 ± 0.9	0.62 ± 0.09

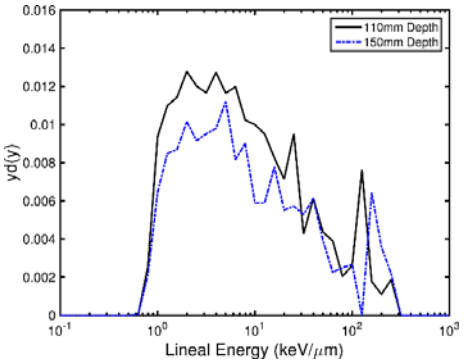

Figure 4. Microdosimetric spectra obtained at depths 110mm and 150mm in water.

Lateral to the Field Edge

Microdosimetric spectra produced from out-of-field acquisitions at each lateral location for depths 25 mm and 80 mm are shown in figure 5 and figure 6, respectively. For these acquisitions, the spectra is characterized by a low lineal energy peak with a higher lineal energy tail. For both depths, the microdosimetric spectra obtained at 10mm out-of-field spans a large range of lineal energies from approximately 0.7 keV/μm to 70 keV/μm, produced by laterally scattered primary protons due to the relatively wide penumbra. At a depth of 80 mm in water, the microdosimetric spectrum for 10 mm out-of-field is naturally broader compared to that at 25 mm depth as the scattered protons have lower energy, and hence higher LET at greater depths. Moving further laterally from the field edge, at 30, 60 and 120 mm, the spectrum is dominated by recoil protons induced by neutrons and are extremely similar for both 25 mm and 80 mm depths.

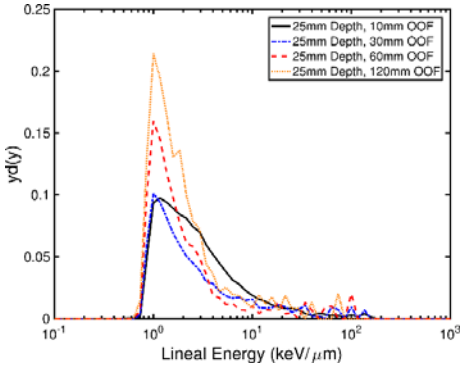

Figure 5. Microdosimetric spectra at 10, 30, 60 and 120 mm laterally out-of-field (OOF) at a depth of 25 mm in water.

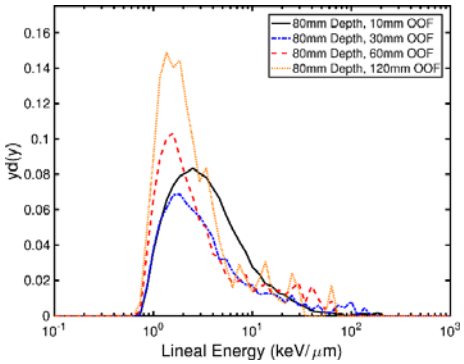

Figure 6. Microdosimetric spectra at 10, 30, 60 and 120 mm laterally out-of-field (OOF) at a depth of 80 mm in water.

Figure 7 shows the $\overline{y_D}$ distributions for out-of-field positions at 25 mm and 80 mm depths in water. Despite the detector being located at significantly different parts along the SOBP profile (see figure 2), the $\overline{y_D}$ distributions are extremely similar. At 10 mm from the field edge, $\overline{y_D}$ increases from approximately 5.8 keV/μm and reaches a maximum of 7.5 and 7.8 keV/μm for 25 mm and 80 mm depths, respectively, followed by a gradual fall-off with distance. Overall, for each lateral location, the $\overline{y_D}$ values at 80 mm depth

are greater than those at 25 mm depth by between 2 - 7%, however agree within experimental error.

The dose-equivalents for each set of out-of-field acquisitions at 25 mm and 80 mm depths are also presented in figure 7. Maximum values were measured at 10 mm from the field edge, reaching values of 3.1 mSv/Gy and 5.3 mSv/Gy at depths 25 mm 80 mm, respectively. For perspective, a total treatment of 60Gy using this field would give a 300mSv dose-equivalent to a point of healthy tissue located 10 mm from the field edge. As expected, the dose-equivalent rapidly falls off with distance from the field edge, converging to approximately 0.04 mSv/Gy at 120 mm out-of-field for both depths.

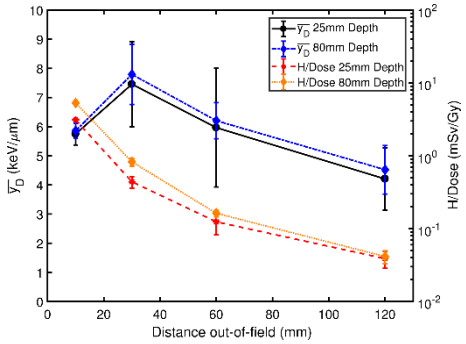

Figure 7. Lateral $\overline{y_D}$ and H distributions for out-of-field acquisitions at 25 mm and 80 mm depths.

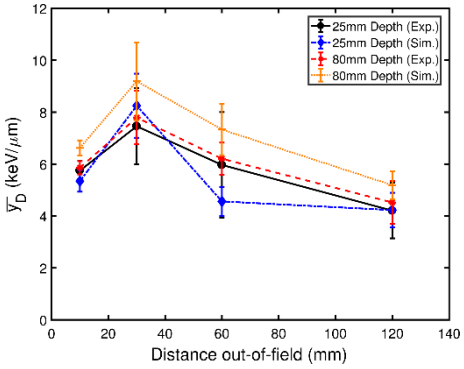

Figure 8. Comparison of simulated and experimental $\overline{y_D}$ values for out-of-field acquisitions at 25 mm and 80 mm depths.

Fig. 8 shows a comparison of the experimental and simulation results for 25mm and 80 mm depths. Good agreement between the experimental and simulation results was observed for 25 mm depth, however at 80 mm, the simulated $\overline{y_D}$ values are slightly higher than the experimental results. This may be explained by a few high LET events which can significantly change the $\overline{y_D}$ value and can lead to substantial $\overline{y_D}$ uncertainties.

Motion Effects in Heavy Ion Therapy

Figure 9 shows a comparison of the microdosimetric spectra when undergoing longitudinal lung motion. A significant difference was observed between the stationary spectra at 148mm (1 mm downstream of the distal edge) and when undergoing lung motion between 141-149mm. When in motion, the edge of the hypothetical critical organ (represented by the microdosimeter) enters the highest LET region of the field, resulting in lineal energy events from carbon ions which dominate the spectra. In the stationary case, lower lineal energy events from neutron interactions dominate. From this observable change in field quality, there would be significantly more *unplanned* damage to the non-target volume in a clinical scenario. This is due to a significantly higher dose and increased $\overline{y_D}$ and RBE_{10} values, as seen in table 2.

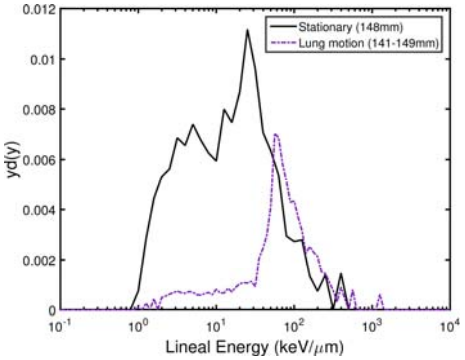

Figure 9. Microdosimetric spectra from stationary and moving acquisitions from depths 148mm, and undergoing lung motion from 141-149mm.

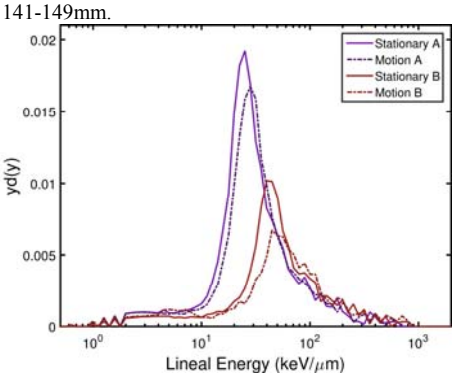

Figure 10. Microdosimetric spectra from stationary and moving acquisitions at points A and B with the bolus (fig. 4).

Figure 10 shows the microdosimetric spectra when the microdosimeter is stationary and when undergoing motion at points A and B (see figure 3) with corresponding $\overline{y_D}$ and RBE_{10} values shown in table 2. At both points, the $\overline{y_D}$ values when undergoing motion were greater the corresponding stationary measurement, showing a relative increase of 9.2% at point A and 13.6% at point B. When undergoing motion, the spectra in both cases shifts towards higher lineal energies due to the contribution of high LET ^{12}C

ions stopping at the end of their range, towards the edge of the bolus. An increase in low lineal energy events was also observed when in motion from point B due to a higher contribution of fragments and neutrons produced from particle interactions further upstream.

Table 2. Dose-mean lineal energy and RBE_{10} for all stationary and motion configurations

Configuration	$\overline{y_D}$ (keV/μm)	RBE_{10}
Lung Motion	96.98 ± 9.57	2.24 ± 0.30
Stationary	31.98 ± 5.11	1.41 ± 0.12
Motion A	48.30 ± 2.46	1.70 ± 0.18
Stationary A	44.22 ± 2.32	1.64 ± 0.16
Motion B	84.34 ± 6.90	2.03 ± 0.25
Stationary B	74.23 ± 4.60	2.00 ± 0.25

CONCLUSIONS

This work has demonstrated two specifics applications of the CMRP high spatial resolution "bridge" μ^+ probe in proton and ^{12}C ion therapy. The small size of the μ^+ probe with SOI microdosimeter has allowed measurements to be taken out-of-field, close to the field edge where critical organs may be in the body during treatment. Conventional detectors such as the tissue-equivalent proportional counter are too large to achieve this and are hence less relevant to predicting secondary cancer effects.

Out-of-field measurements with the SOI microdosimeter in a proton PBS field have been carried out for the first time and revealed an interesting y_D distribution laterally to the field at different depths. For both depths at 10 mm from the field edge, the microdosimetric spectra is dominated by laterally scattered primary protons from the nozzle, resulting in a relatively low y_D. Moving further out between 30 mm – 120 mm from the field edge, $\overline{y_D}$ increases due to the fast neutron contribution, followed by a gradual fall-off with distance. The measured $\overline{y_D}$ distributions at 25 mm depth are in slightly better agreement with predicted Monte Carlo simulations than 80 mm depth due to possible lack of statistics that may effect neutron spectra and lead to slightly increased probability of Si(n, α) events. The dose-equivalent for proton PBS delivery systems shows significant differences to values obtained for fields delivered using non-scanning systems[9]

The μ^+ probe with SOI "bridge" microdosimeter also proved to be useful for studying the effects of target motion in ^{12}C ion therapy. Large differences in microdosimetric spectra and RBE_{10} were observed at stationary points and for motion along different kinds of trajectories. Obtained results show that this device is suitable for investigating interplay effects by mimicking organ motion due to its lightweight construction and the stable microphonic properties of the probe front-end.

ACKNOWLEDGEMENTS

This research has been conducted with financial support of the Australian Government Research Training Program Scholarship and AINSE Limited PGRA.

REFERENCES

1. J. Brenner and E. J. Hall, *Secondary neutrons in clinical proton radiotherapy: A charged issue*, Radiother. Oncol. **86**, 165–170 (2008).
2. J. Lomax, *Charged particle therapy: the physics of interaction*, Cancer J. **15**, 285–91 (2009).
3. E. Pedroni *et. al.*, *The PSI Gantry 2: a second generation proton scanning gantry*, Z. Med. Phys. **14**, 25–34 (2004).
4. H. M. Kooy *et. al.*, *A Case Study in Proton Pencil-Beam Scanning Delivery*, Int. J. Radiat. Oncol. Biol. Phys. **76**, 624–630 (2010).
5. U. Schneider *et. al.*, *Secondary neutron dose during proton therapy using spot scanning*, Int. J. Radiat. Oncol. Biol. Phys. **53**, 244–251 (2002).
6. X. Yan *et. al.*, *Measurement of neutron dose-equivalent to proton therapy patients outside of the proton radiation field*, Nucl. Instr. Meth. Phys. Res. B **476**, 429–434 (2002).
7. A. Wroe, A. Rosenfeld, and R. Schulte, *Out-of-field dose-equivalents delivered by proton therapy of prostate cancer*. Med. Phys. **34**, 3449–3456 (2007).
8. A. Wroe *et. al.*, *Out-of-Field Dose-equivalents Delivered by Passively Scattered Therapeutic Proton Beams for Clinically Relevant Field Configurations*, Int. J. Radiat. Oncol. Biol. Phys. **73**, 306–313 (2009).
9. B. Clasie *et. al.*, "Assessment of out-of-field absorbed dose and equivalent dose in proton fields." Med. Phys. 37, 311–321 (2010).
10. E. J. Hall, *Intensity-Modulated Radiation Therapy, Protons, And The Risk Of Second Cancers (Int. J. Radiat. Oncol. Biol. Phys. 2006;65:1-7)*, Int. J. Radiat. Oncol. Biol. Phys. **66**, 1593–4; author reply 1595 (2006).
11. B. Gottschalk, *Neutron dose in scattered and scanned proton beams: In regard to Eric J. Hall (Int. J. Radiat. Oncol. Biol. Phys. 2006;65:1-7)*, Int. J. Radiat. Oncol. Biol. Phys. **66**, 1594 (2006).
12. D. D. Ruysscher *et. al*. *Tumour Movement in Proton Therapy: Solutions and Remaining Questions: A Review*, Cancers **7**, 1143–1153, Web (2017).
13. A. Gemmel *et. al*., *Experimental verification of motion mitigation of discrete proton spot scanning by re-scanning*, Phys. Med. Biol. **56**, 8555–8572 (2013).
14. Y. Kase *et. al.*, *Microdosimetric approach to NIRS-defined biological dose measurement for carbon-ion treatment beam*, J. Radiat. Res. **52**, 59-68 (2011).
15. M. Z. Harald H. Rossi, *Microdosimetry and Its Applications*, Springer Berlin Heidelberg (1996).
16. A. B. Rosenfeld *et. al.*, *Solid state microdosimetry in hadron therapy*, Radiat. Prot. Dosimetry **101**, 431–434 (2002).

17. L. T. Tran *et. al.*, *3D-mesa 'bridge' silicon microdosimeter: Charge collection study and application to RBE studies in ^{12}C radiation therapy*, IEEE. Trans. Nucl. Sci. **62**, 504–511 (2015).
18. L. Tran *et. al.*, *3D silicon microdosimetry and RBE study using ion of different energies*, IEEE. Trans. Nucl. Sci. **62**, 3027–3033 (2015).
19. International Committee on Radiation Units and Measurements, *ICRU Report 40* (1986).
20. D. Bolst *et. al.*, *Correction factors to convert microdosimetry measurements in silicon to tissue in ^{12}C ion therapy*, Phys. Med. Biol. **62**, 2055-2069 (2017).
21. L. Tran *et. al., Characterisation of proton pencil beam scanning and passive beam using a high spatial resolution solid state microdosimeter,* Med. Phys, in press.